PHYSICAL REVIEW D **94,** 116008 (2016)

Chiral symmetry restoration for the large-N pion gas

Santiago Cortés,[1,*] A. Gómez Nicola,[2,†] and John Morales[3,‡]
[1]*Departamento de Física, Univ. de Los Andes, 111711 Bogotá, Colombia*
[2]*Departamento de Física Teórica II. Univ. Complutense, 28040 Madrid. Spain*
[3]*Departamento de Física, Univ. Nacional de Colombia, 111321 Bogotá, Colombia*
(Received 3 October 2016; published 21 December 2016)

We analyze chiral restoration within the $O(N+1)/O(N)$ nonlinear sigma model for large N as an effective theory for low-energy QCD at finite temperature T. The free energy is constructed diagrammatically to $\mathcal{O}(TM^3)$ in the pion mass expansion, which allows us to derive the quark condensate and the scalar susceptibility in the chiral limit. At this order, we do not have to deal with renormalization, either from divergences from mass tadpoles or from those of higher order loop contributions. Our results for the critical behavior are consistent with expectations from lattice analysis and with previous works where the susceptibility is saturated by the thermal $f_0(500)$ pole.

DOI: 10.1103/PhysRevD.94.116008

I. INTRODUCTION

The study of hadronic properties at finite temperature T is one of the theoretical ingredients needed to understand the behavior of matter created in relativistic heavy ion collision experiments, such as those in RHIC and LHC (ALICE). In particular, the QCD transition involving chiral symmetry restoration and deconfinement plays a crucial role, as is clear from the many recent advances of lattice groups in the study of the phase diagram and other thermodynamical properties [1–4]. For vanishing baryon chemical potential, the QCD transition is a crossover for $2+1$ flavors with physical quark masses, the transition temperature being about $T_c \sim 150$–160 MeV, determined by the vanishing behavior of the quark condensate and the peak of the scalar susceptibility. In the chiral limit it becomes a second-order phase transition consistent with the $O(4)$-model universality class [5,6], which is supported in lattice simulations by the mass and temperature scaling of thermodynamical quantities as well as chiral partner degeneration [2,3]. The expected reduction in the transition temperature from the physical mass case to the chiral limit one based on those analysis is about 15%–20% [3].

From the theoretical side, it is therefore important to provide solid analysis of this chiral restoration pattern based on effective theories, given the limitations of perturbative QCD at those temperature scales. Such effective description should start from a proper understanding of the lightest component, i.e., the pion gas. Pions are actually the most abundant particles after a heavy ion collision and most of their properties from hadronization to thermal freeze-out can be reasonably described within the temperature range where effective theories are applicable. In fact, approaches based on effective theories for the lightest mesons provide a good description of the physics involved, especially in what concerns the effect of the lightest resonances, as we discuss below. A more accurate treatment of thermodynamic quantities near T_c requires including heavier degrees of freedom, which can be efficiently achieved through the hadron resonance gas framework [7,8].

A systematic and model-independent framework that takes into account the relevant light meson degrees of freedom and their interactions is chiral perturbation theory (ChPT) [9]. The effective ChPT Lagrangian is constructed as a derivative and mass expansion $\mathcal{L} = \mathcal{L}_{p^2} + \mathcal{L}_{p^4} + \cdots$, where p denotes generically a meson energy scale compared to the chiral scale $\Lambda_\chi \sim 1$ GeV. The lowest order Lagrangian $\mathcal{L}_{p^2}$ is the nonlinear sigma model (NLSM). Thus, chiral restoring behavior is qualitatively obtained within ChPT through the vanishing quark condensate for different orders [10], although a critical description is not obtained in the chiral limit. Despite the model-independent character of the ChPT predictions for chiral restoration, the low-T nature of this theory implies a continuous behavior for order parameters and susceptibilities, even in the chiral limit. Thus, the quark condensate is a dropping continuous function around the critical point and the scalar susceptibility grows also continuously. In addition, ChPT is unable to describe resonant states, which play a crucial role in the description of the hadronic medium. Some of these limitations are improved within the unitarized framework at finite temperature [11,12], which provides an accurate description of several effects of interest in a heavy ion environment, such as thermal resonances and transport coefficients [13]. It provides also a novel understanding of the role of the $\sigma/f_0(500)$ $I=J=0$ thermal pole (a broad resonant state) in chiral symmetry restoration. Thus, the scalar susceptibility saturated with this σ-like state within the so-called inverse amplitude method (IAM) unitarization develops a maximum near T_c [14]

*js.cortes125@uniandes.edu.co
†gomez@ucm.es
‡jmoralesa@unal.edu.co

compatible with lattice data and chiral partners in the scalar-pseudoscalar sector are understood through degeneration of correlators and susceptibilities. The role of the $f_0(500)$ state for chiral restoration could become more complicated if its possible tetraquark component is also considered at finite temperature [15].

A complementary approach is the large-N one, where N is the number of light Nambu-Goldstone bosons (NGB). Within this framework, the lowest order chiral effective Lagrangian for low-energy QCD is the $O(N+1)/O(N)$ NLSM, whose corresponding symmetry breaking pattern is $O(N+1) \to O(N)$. As we have just commented, the latter is believed to take place in chiral symmetry restoration for $N=3$, since $O(4)$ and $O(3)$ are respectively isomorphic to the isospin groups $SU_L(2) \otimes SU_R(2)$ and $SU_V(2)$. In this limit, many of the features discussed above arise naturally. For instance, the pion scattering amplitude generates the $f_0(500)$ resonance in accordance with scattering and pole data. When extended at finite temperature, thermal unitarity holds exactly and the thermal pole gives rise to a saturated scalar susceptibility diverging in the chiral limit at the critical temperature as a second-order phase transition [16]. Within a similar context, it is worth mentioning also recent large-N analysis in the vector $O(N)$ model regarding the σ spectral properties at finite T [17].

The large-N framework for the NLSM has been analyzed in earlier works under various approximations. At $T=0$, functional methods were developed in [18]; the scattering amplitude, including its renormalizability, was studied in the chiral limit in [19] and to leading order in mass corrections in [20]. At finite temperature, apart from the previously mentioned work [16], the free energy and the quark condensate within a saddle-point approximation for the auxiliary field were analyzed in [21]. Other studies in the chiral limit that also utilize functional methods [22] provide a chiral restoring analysis and the T-dependence of the pion decay constant [23]. A later work [24] studied the NLSM as the infinite coupling limit of the $O(N)$ vector model, their results for the NLO pressure in the chiral limit not being fully consistent with those in [22]. Various renormalization-group studies of the critical properties of this model were compiled in [25].

In this work we analyze the leading large-N contributions to the quark condensate and the scalar susceptibility, derived diagrammatically from the partition function or the free energy. Since we are mostly interested in the study of the critical behavior, we restrict ourselves to the leading order in the expansion around the chiral limit, which has the additional advantage of yielding results that are not to be renormalized. The scalar susceptibility and the analysis of the critical behavior are new from this work. In addition, another motivation for the present study and a prominent difference with respect to previous analysis is that we work directly within the diagrammatic approach to the partition function, identifying the dominant contributions to the free energy. Thus, that approach does not introduce additional assumptions within the auxiliary field method, such as saddle-point approximations, but requires a careful evaluation of the diagrams and effective vertices involved. In fact, for the susceptibility analysis we deal with a resummation of an infinite set of closed ring diagrams, which confirm qualitatively the analysis performed previously in terms of pion scattering and the thermal $f_0(500)$ saturation. That comparison is also another motivation for the present work. We need to calculate the large-N free energy up to order TM^3 in order to extract properly the leading order susceptibility near the chiral limit, which actually means going beyond previous analysis of the NLSM for large N. In this sense, our present study aims to set up the correct diagrammatic framework for future analysis beyond the chiral limit. The paper is organized as follows: we present our main formalism in Sec. II, the detailed diagrammatic analysis is performed in Sec. III, and the results are presented in Sec. IV, where we compare the obtained critical behavior with previous theoretical approaches, as well as with lattice results for critical exponents.

II. FORMALISM AND CONVENTIONS

We start from the Lagrangian of the nonlinear $S^N = O(N+1)/O(N)$ model with a explicit symmetry breaking term that generates the pion mass [20],

$$\begin{aligned}\mathcal{L}_{NLSM} &= \frac{1}{2}\left[\delta_{ab} + \frac{1}{NF^2}\frac{\boldsymbol{\pi}_a\boldsymbol{\pi}_b}{1-\boldsymbol{\pi}^2/NF^2}\right]\partial_\mu\boldsymbol{\pi}^a\partial^\mu\boldsymbol{\pi}^b \\ &\quad + NF^2M^2\sqrt{1-\frac{\boldsymbol{\pi}^2}{NF^2}} \\ &= NF^2M^2 + \frac{1}{2}\partial_\mu\boldsymbol{\pi}^a\partial^\mu\boldsymbol{\pi}^a - \frac{1}{2}M^2\boldsymbol{\pi}^2 \\ &\quad + \frac{1}{2NF^2}\boldsymbol{\pi}^a\boldsymbol{\pi}^b\partial_\mu\boldsymbol{\pi}_a\partial^\mu\boldsymbol{\pi}_b f\left(\frac{\boldsymbol{\pi}^2}{NF^2}\right) \\ &\quad - \frac{M^2}{8NF^2}(\boldsymbol{\pi}^2)^2 g\left(\frac{\boldsymbol{\pi}^2}{NF^2}\right),\end{aligned} \tag{1}$$

with $\boldsymbol{\pi}^2 = \sum_{a=1}^N \boldsymbol{\pi}_a\boldsymbol{\pi}^a$ and M^2 and $\sqrt{N}F$ being respectively the pion mass and the pion decay constant in the chiral limit. Here we have explicitly separated the kinetic free Lagrangian and written the interaction part, with and without derivatives, in terms of the functions,

$$\begin{aligned}f(x) &= \frac{1}{1-x} = \sum_{k=0}^{\infty} x^k, \\ g(x) &= -\frac{8}{x^2}\left[\sqrt{1-x} - 1 + \frac{x}{2}\right] \\ &= -8\sum_{k=0}^{\infty}(-1)^k\binom{1/2}{k+2}x^k = 1 + \frac{x}{2} + \frac{5}{16}x^2 + \cdots,\end{aligned} \tag{2}$$

where $\binom{\alpha}{n} = \frac{1}{n!}\alpha(\alpha-1)\cdots(\alpha-n+1)$. Both $f(x)$ and $g(x)$ are normalized so that the leading order in the $1/F^2$ ChPT expression ($x \to 0$) corresponds to $f = g = 1$. Similar functions are used in the analysis of pion scattering in the massive case at $T = 0$ within the auxiliary field method [20].

The free energy from which all the thermodynamic variables can be extracted is given by

$$z(M,T) = -T\lim_{V\to\infty}\frac{1}{V}\log Z(M,T),$$
$$Z(M,T) = \int d\boldsymbol{\pi}\exp\int_T \mathcal{L}[\boldsymbol{\pi}], \tag{3}$$

where $Z(M,T)$ is the QCD partition function in the pionic sector, hence expected to be dominant at low and moderate temperatures, and $\int_T \equiv \int_0^\beta d\tau\int d^3\vec{x}$, $\beta = 1/T$, $\mathcal{L}[\boldsymbol{\pi}] = \mathcal{L}_{NLSM}[\boldsymbol{\pi}] + \cdots$, the dots indicating higher order Lagrangians in derivatives and masses, which eventually have to be included to renormalize the theory, within the same approach followed in previous works [9,10,16,19,20].

The light quark condensate behaves as an order parameter for chiral symmetry restoration in the chiral limit,

$$\langle\overline{q}q\rangle(M,T) = \frac{\partial z(M,T)}{\partial m_q} = 2B_0\frac{\partial z(M,T)}{\partial M^2}, \tag{4}$$

where m_q is the light quark mass, $\overline{q}q = \sum_{i=1}^{N_f}\overline{q}_i q_i$ with N_f being the number of light flavors, and we have used the standard relation between the NGB mass and the quark mass $M^2 = 2B_0 m_q$, related also to the $T = 0$ quark condensate in the chiral limit $\langle\overline{q}q\rangle(T=0) = -2NF^2B_0$.

The quark condensate correlator defines the scalar susceptibility, namely,

$$\begin{aligned}\chi_S(M,T) &= -\frac{\partial}{\partial m_q}\langle\overline{q}q\rangle(M,T)\\ &= -\frac{\partial^2}{\partial m_q^2}z(M,T) = -4B_0^2\frac{\partial^2}{\partial(M^2)^2}z(M,T)\\ &= \int_T d^4x[\langle\mathcal{T}(\overline{q}q)_l(x)(\overline{q}q)_l(0)\rangle_T - \langle\overline{q}q\rangle^2(T)].\end{aligned} \tag{5}$$

An important comment is that throughout this work, we are interested only in the chiral limit $M \to 0^+$, which, as explained above, should capture the essential features of the chiral phase transition, both for the quark condensate and for the scalar susceptibility. However, from their previous definitions (4) and (5), we see that it is necessary to keep M^2 finite and send it to 0 only after differentiation. Thus, we consider the large-N leading contribution for finite mass and then we keep only the relevant terms in the M^2 expansion near the chiral limit. This is a distinctive feature with respect to previous large-N NLSM analysis at finite T, which analyzes $z(T)$ within the limit of massless pions, but not its M^2 corrections [22,24], particularly relevant for the case of χ_S, since from its divergent nature near the transition it is indeed expected to behave as an $\mathcal{O}(M^{-1})$ quantity [26,27], which we also obtain in this approach by keeping the relevant M^3 terms.

In the following analysis, the free-energy density is expressed in terms of different thermal functions. Following the same notation as in [10], we define $g_k(M,T)$ satisfying $g_{k+1}(M,T) = -\frac{\partial}{\partial M^2}g_k(M,T)$ and whose expansion in M/T reads (we keep the terms relevant for this work)

$$\begin{aligned}g_0(M,T) = \frac{\pi^2}{45}T^4\Bigg[1 - 15\left(\frac{M}{2\pi T}\right)^2 + 60\left(\frac{M}{2\pi T}\right)^3\\ + \mathcal{O}\left(\left(\frac{M}{2\pi T}\right)^4\log\left(\frac{M}{2\pi T}\right)\right)\Bigg],\end{aligned} \tag{6}$$

$$g_1(M,T) = \frac{T^2}{12}\left[1 - 3\frac{M}{\pi T} + \mathcal{O}\left(\left(\frac{M}{2\pi T}\right)^2\log\left(\frac{M}{2\pi T}\right)\right)\right], \tag{7}$$

$$g_2(M,T) = \frac{T}{8\pi M} + \mathcal{O}\left(\log\left(\frac{M}{2\pi T}\right)\right). \tag{8}$$

The above g_i functions arise naturally from thermal parts of loop functions. Thus, defining $G_1(M,T) = G(x=0)$ as the tadpole function with G being the free pion propagator, we have

$$\begin{aligned}G_1(M,T) &= T\sum_n\int\frac{d^3\vec{q}}{(2\pi)^3}\frac{1}{\omega_n^2 + |\vec{q}|^2 + M^2}\\ &= G_1(M,0) + g_1(M,T),\\ G_1(M,0) &= M^2\left[(4\pi)^{-D/2}\Gamma\left(1-\frac{D}{2}\right)\mu^{D-4} + \frac{1}{16\pi^2}\log\frac{M^2}{\mu^2}\right],\end{aligned} \tag{9}$$

with $\omega_n = 2\pi nT$ being the Matsubara frequencies, μ the renormalization ChPT scale, and Γ the Euler gamma function. We follow the same notation as in [9].

The g_2 function corresponds to the thermal part of the scattering loop with zero external momenta,

$$\begin{aligned}G_2(M,T) &= T\sum_n\int\frac{d^3\vec{q}}{(2\pi)^3}\frac{1}{(\omega_n^2 + |\vec{q}|^2 + M^2)^2}\\ &= -\frac{d}{dM^2}G_1(M,T) = G_2(M,0) + g_2(M,T).\end{aligned} \tag{10}$$

Similarly, we define the loop function

$$G_k(M,T) = T\sum_n \int \frac{d^3\vec{q}}{(2\pi)^3}\frac{1}{(\omega_n^2+|\vec{q}|^2+M^2)^k} = \frac{1}{(k-1)!}\left(-\frac{d}{dM^2}\right)^{k-1} G_1(M,T) = G_k(M,0)+\frac{1}{(k-1)!}g_k(M,T) = \frac{TM^3}{8\pi}\frac{(2k-5)!!}{(k-1)!2^{k-2}}\frac{1}{M^{2k}}\left[1+\mathcal{O}\left(\frac{M}{T}\right)\right] \quad \text{for } k\geq 3, \tag{11}$$

where we have extracted the leading order in the T/M expansion from the asymptotic expansion (7).

III. LARGE-N AND MASS EXPANSION

In order to identify the leading order contribution in the large-N limit for fixed mass M^2, it is useful to examine the different possible terms for a given number of vertices, i.e., to a certain order in the expansion of the interaction part of the Lagrangian (1) in the free energy (3). Thus, we first extract the constant term $z_c = -NF^2M^2$, which is $\mathcal{O}(N)$, and we denote by z_n the leading contribution for n vertices at large N for fixed M^2. The contribution with zero vertices is that coming from the free kinetic pion part of the NLSM Lagrangian (1); this corresponds to the free partition function of an N-component massive boson gas,

$$z_0(M,T) = -\frac{N}{2}\left[(4\pi)^{-D/2}\Gamma\left(-\frac{D}{2}\right)M^D + g_0(M,T)\right], \tag{12}$$

which is also $\mathcal{O}(N)$. The contributions z_c and z_0 are given by diagrams (a) and (b) in Fig. 1, respectively.

We also keep the space-time dimension $D = 4-\epsilon$ in the dimensional regularization scheme. The free energy is divergent and needs renormalization, as it is discussed in detail within the ChPT expansion in [10]. Renormalization within the large-N framework can also be carried out by including suitable higher order Lagrangians in derivatives and masses. This is reviewed for the scattering amplitude at $T=0$ in [19,20] and for $T\neq 0$ in [16]. At the order considered in this work, as we see, the dominant contribution is finite, so we do not need to implement explicitly such a renormalization procedure.

The one-vertex contribution corresponds to the first order in the expansion of the interaction Lagrangian in (1). In the mass vertex term, i.e., the one with the g function, we get the maximal contribution in N by contracting all pion pairs with the same isospin indices, so that $\boldsymbol{\pi}^a\boldsymbol{\pi}_a \to NG_1(M,T)$ with G_1 in (9). Therefore, we have to sum all tadpole insertions in the vertex as given by the function g in the Lagrangian, which we attain by defining an effective vertex as indicated in Fig. 2.

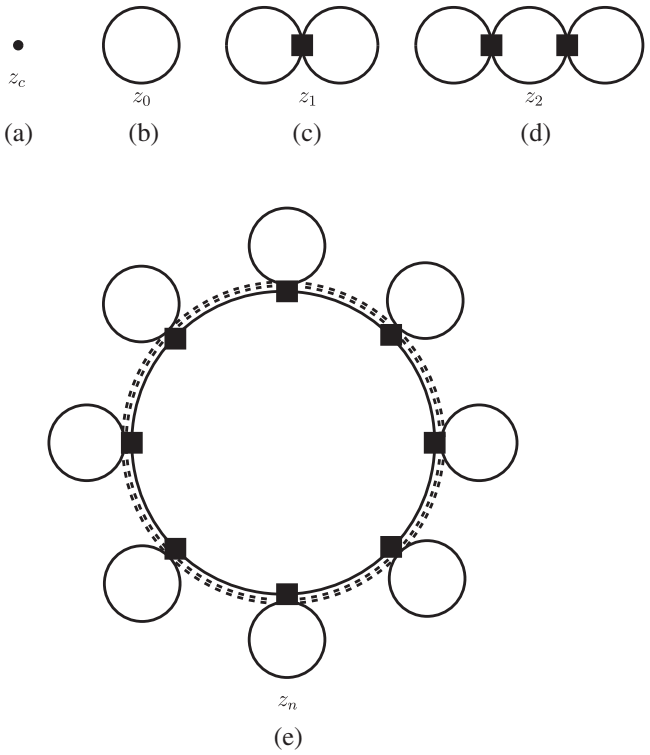

FIG. 1. Diagrams contributing to the free energy to leading order in N and up to $\mathcal{O}(TM^3)$. The black squares denote the effective vertex depicted in Fig. 2. The different contributions (a)–(e) are explained in the main text. The dashed lines in (e) indicate multiple insertions of this vertex along the central loop

On the other hand, one realizes that contractions involving the interaction derivative term in the Lagrangian [the term proportional to the function f in (1)] give always subdominant contributions in N since $\boldsymbol{\pi}^a\partial_\mu\boldsymbol{\pi}_a \to \partial_\mu G_1|_{x=0} = 0$ by parity, so those contributions are $\mathcal{O}(1)$ in the large-N expansion of the free energy.

We point out that the combinatoric factors shown in Fig. 2 remain the same as those obtained from the $1/N$ expansion of the mass vertex in (1). This is because our analysis, albeit diagrammatical, is not describing any specific scattering process as in previous analysis [16] but closed diagrams for the free energy, so we do not have to consider extra factors in the resummation given by the function $g(G_1/F^2)$. Another significant difference with the scattering case is that here derivative vertices do not show up to leading order. Thus, we obtain for the large-N leading one-vertex contribution to the free energy

$$z_1(M,T) = \frac{N}{8}\frac{M^2}{F^2}G_1^2(M,T)\,g\left[\frac{G_1(M,T)}{F^2}\right] + \mathcal{O}(N^0) = -NM^2F^2\left\{h\left(\frac{T^2}{12F^2}\right) - \frac{MT}{4\pi F^2}h'\left(\frac{T^2}{12F^2}\right)\right\} + \mathcal{O}[M^4\log M, N^0], \tag{13}$$

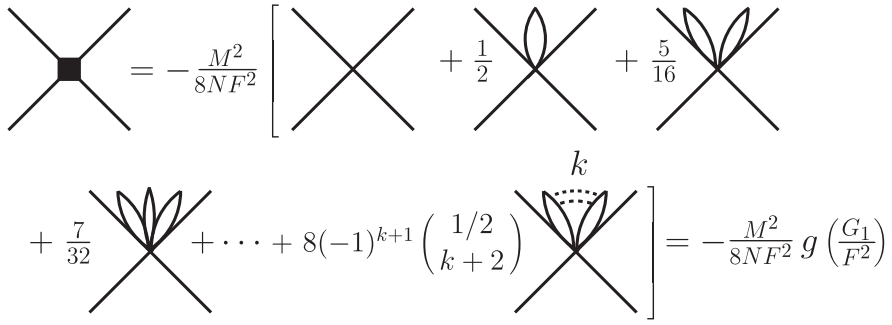

FIG. 2. Effective mass vertex. Dashed lines in the last diagram indicate the multiple insertions of pion tadpoles coming from contractions of pairs of extra legs.

according to (7) and (9), with $h(x) = -(1/8)x^2 g(x)$.[1] The above contribution z_1 corresponds to the connected diagram (c) in Fig. 1. The topology of this diagram is the same as in ChPT [10] but here effective mass vertices enter and derivative vertices are absent.

For two vertices, following the above considerations, the dominant contribution in N, which is again $\mathcal{O}(N)$, is obtained by taking the two vertices as the two mass effective vertices of Fig. 2. The corresponding connected diagram is shown in Fig. 1(d). Thus, those effective vertices count as $1/N$ each, the external bubbles connected to the vertex also count as N, and the internal bubble connecting the two vertices counts an additional $N = \delta_{ab}\delta^{ab}$ coming from $\boldsymbol{\pi}^2(x)\boldsymbol{\pi}^2(y)$. Any other combination is subleading, including the derivative vertices in (1). Hence, even if the $\boldsymbol{\pi}^2$ contractions in $f(x)$ are taken maximally in N, since $\partial\boldsymbol{\pi}_a\boldsymbol{\pi}^a$ cannot be contracted at the same point one ends in diagram (d) in Fig. 1 with the structure $N\delta^{ab}\delta_{ac}\delta^c_b = N^2$ for one mass vertex and one derivative vertex and $\delta^{ab}\delta_{ac}\delta_{bd}\delta^{cd} = N$ for two derivative vertices, instead of the N^3 structure of the two mass vertices. Following the same arguments, other topologies of diagrams considered in the ChPT expansion [10] are subdominant for large N at finite mass, like diagram (a) in Fig. 3.

To calculate the dominant z_2 contribution from Fig. 1(d), we have to include a combinatoric factor accounting for all the possible ways to choose a $\boldsymbol{\pi}^2$ in each vertex that is to be connected with the other vertex. Thus, at each vertex there is an additional $k_i + 2$ factor, where k_i is the integer labeling the power $(\boldsymbol{\pi}^2)^{k_i+2}$ at vertex $i = 1, 2$. Hence, we end up with a modified effective vertex function for that diagram, namely,

$$\frac{M^2}{NF^2}\sum_{k=0}^{\infty}(-1)^k(k+2)\binom{1/2}{k+2}x^k = -\frac{1}{2}\frac{M^2}{NF^2}\frac{\tilde{g}(x)}{x},$$
$$\tilde{g}(x) = \frac{1}{4}\frac{d}{dx}[x^2 g(x)] = -2h'(x) = \frac{1}{\sqrt{1-x}} - 1. \tag{14}$$

[1]Note that the function $h(x)$ corresponds to $-g^2(x)$ in [20].

In addition, we have to multiply by 2 from the two ways to contract $\pi^2(x)\pi^2(y)$ and by $1/2$ from the Lagrangian expansion, so that the leading $\mathcal{O}(N)$ term for z_2 is

$$z_2(M,T) = -\frac{NM^4}{4}\left[\tilde{g}\left(\frac{G_1(M,T)}{F^2}\right)\right]^2 G_2(M,T) + \mathcal{O}(N^0)$$
$$= -\frac{NM^3T}{32\pi}\left[\tilde{g}\left(\frac{T^2}{12F^2}\right)\right]^2 + \mathcal{O}(M^4\log M, N^0) \tag{15}$$

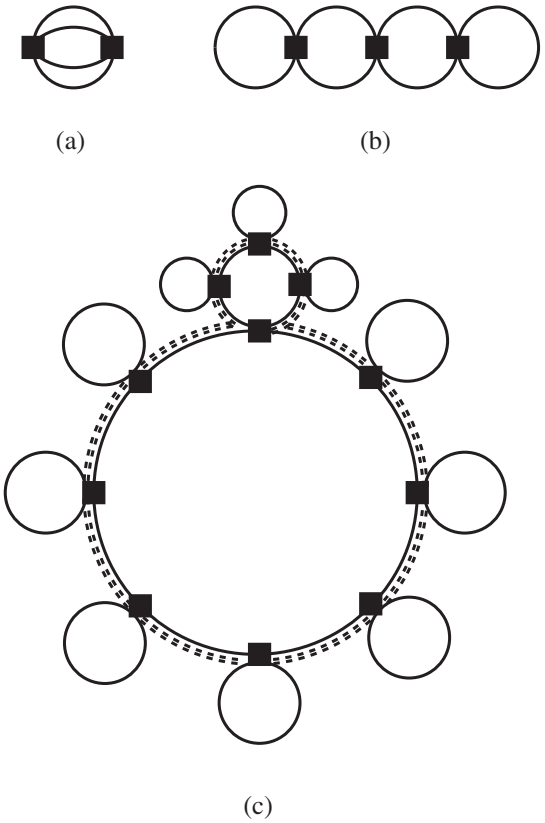

FIG. 3. Different examples of subleading diagrams. (a) is subleading in the large-N expansion for fixed M, while (b) and (c) are of leading $\mathcal{O}(N)$ order but subleading in the M^2 expansion.

with $G_2(M,T)$ in (10) and using the expansions (7) and (8) around the massless limit.

Now, for three or more vertices n, following the previous arguments, the dominant connected diagrams are those with only effective mass vertices and $n+1$ bubbles. Those bubbles can be either closed around one of the vertices or connecting a subset of them, so that two given vertices are connected at most with two lines. Examples of these general $\mathcal{O}(N)$ foam or superdaisy-type diagrams [28,29] are diagram (e) in Fig. 1 and diagrams (b) and (c) in Fig. 3.

However, a crucial point of our present approach is that only a subclass of those foam diagrams is dominant to leading order in the M^2 expansion, namely, the ring or daisy diagrams of the type depicted in Fig. 1. To understand this, note first that any of those generic diagrams contains a product of the type $G_1^{k_1}G_2^{k_2}\cdots G_n^{k_n}$, multiplied by the corresponding effective vertices (which are functions of G_1 only), with $\sum_{i=1}^{n} k_i = n+1$ being the number of loops and G_k given in (11). Hence, we see that the minimum power of M in a foam diagram is obtained when setting k_1 to its maximum allowed value, which is $k_1 = n$ and hence $k_n = 1$, which corresponds to the loop function G_n connecting those n single bubbles, and the other $k_i = 0$. Including also the effective vertices described above, that combination corresponds to the ring diagrams depicted in Fig. 1(e), whose M^2 counting is then $(M^2)^n G_n = \mathcal{O}(TM^3)$ times a function of $T^2/12F^2$, near the chiral limit. Other foam diagrams are subleading, like diagram (b) in Fig. 3, whose leading order mass dependence comes from $(M^2)^3 G_2^2$ and then it becomes $\mathcal{O}(M^4)$ times a function of $T^2/12F^2$. Similar arguments can be followed for other subleading diagrams like diagram (c) in Fig. 3, whose leading M power is set by the functions $G_{k>1}$. We recall that the dominance of ring diagrams near the infrared region is a known feature of thermal field theory [30] and allows us precisely to extract the $\mathcal{O}(TM^3)$ term needed to calculate the leading order of the scalar susceptibility.

In addition, and as announced above, to this leading order all the results are finite, since the $T=0$ corrections are subleading. Therefore, at this level of approximation we do not need to discuss the renormalization details of the calculation in terms of the infinite set of coupling constants arising from higher order Lagrangians [16,19,20]. Within that standard large-N approach, we can consider then that those low-energy constants of higher order are subleading. We just keep in mind that they may introduce subleading corrections to our expressions, which for instance could modify numerically the transition temperature, as we discuss below.

The energy density up to $\mathcal{O}(TM^3)$ in the large-N limit is obtained then by summing all ring diagrams, taking into account that we have to multiply by the following: (i) $[-M^2\tilde{g}(G_1/F^2)/(2N)]^n$ from the modified effective vertex (14), counting all the ways to take in each effective vertex the two pion lines shared with the adjacent vertices, and where we have taken into account that there is a tadpole function G_1 attached to every vertex in the ring diagrams; (ii) by 2^n for the two possible ways to take those shared lines in every link; (iii) by $(1/n!)$ from the series expansion of the interaction Lagrangian; (iv) by $(n-1)!/2$, which are the topologically different ways of sorting n points in a circle; and (v) by N^{n+1} from the loops. Finally we obtain

$$\begin{aligned} z(M,T) &= z_c + \sum_{n=0}^{\infty} z_n(M,T) \\ &= -N\frac{\pi^2 T^4}{90} - NM^2F^2\left\{1 - \frac{T^2}{24F^2} + h\left(\frac{T^2}{12F^2}\right)\right\} \\ &\quad - \frac{NM^3T}{8\pi}\left\{\frac{2}{3} - 2h'\left(\frac{T^2}{12F^2}\right)\right. \\ &\quad \left. + H\left[-\frac{1}{2}\tilde{g}\left(\frac{T^2}{12F^2}\right)\right]\right\} + \mathcal{O}[M^4\log M, N^0], \end{aligned} \tag{16}$$

where $H(x) = x^2 + 2\sum_{n=3}^{\infty}\frac{(2n-5)!!}{n!}x^n = -\frac{2}{3}(1-3x-\sqrt{1-2x}+2x\sqrt{1-2x})$. The combinatoric factor given here resembles that obtained for a finite-temperature effective Higgs potential in [31].

We remark that the result (16) is meaningful only as an expansion around the chiral limit $M \to 0^+$ so we can extract the leading order for the quark condensate and the scalar susceptibility in that limit. Although the mass expansion performed here could yield mass corrections to the free energy, quark condensate, and scalar susceptibility, we must be careful at this point. The M expansion that we have carried out here comes from two different dimensionless parameters, namely, M/T and M/F. Thus, while we expect the behavior of thermal functions to be dominated by the chiral limit contribution in the high temperature regime $T \gg M$, M/F is a pure $T=0$ parameter coming from the mass vertex in the Lagrangian. Therefore, mass corrections might not be reliable for physical masses. A related complication introduced by the large-N resummation is that, as shown above, from z_2 onwards the effective vertex gives rise actually to $M^2\tilde{g}(G_1/F^2)$, with $\tilde{g}$ given in (14), which may introduce spurious divergences near T_c when keeping a finite mass M. For these reasons, we stick here to the strict chiral limit $M \to 0^+$ since it ensures that those two dimensionless scales can be treated as perturbatively equivalent. Thus, we keep only the M^0 term in (17) for the condensate and the M^{-1} term for the scalar susceptibility. In this work we are interested in the critical behavior of the large-N expansion and, therefore, it makes sense to restrict to the chiral limit as a first approximation to the problem. A proper treatment of finite mass effects within the large-N expansion requires, in principle, summing all types of foam diagrams like that in Fig. 3(c).

IV. QUARK CONDENSATE AND SCALAR SUSCEPTIBILITY: RESULTS AND DISCUSSION

From the analysis of the previous section, we can easily extract the quark condensate in the chiral and large-N limits, from (4) and (16),

$$\frac{\langle\bar{q}q\rangle(M,T)}{\langle\bar{q}q\rangle(M,0)}=\sqrt{1-\frac{T^2}{T_c^2}}+\mathcal{O}(M,1/N). \tag{17}$$

where we denote by $T_c^2=12F^2$ the temperature at which the quark condensate vanishes, and $\langle\bar{q}q\rangle(M,0)=-2NF^2B_0+\mathcal{O}(M^2\log M)$. Note that, according to our previous arguments, only the M^2 term in (16) contributes to the leading order displayed in (17). The result (17) is certainly expected from the chiral limit analysis in [22], where the same temperature dependence is found for the scaling of the effective sigma field $\langle\sigma\rangle(T)/\langle\sigma\rangle(0)$. Although the identification $\langle\sigma\rangle\leftrightarrow\langle\bar{q}q\rangle$ is very natural from the viewpoint of the quark model assignment, note that within our present approach we do not need to introduce any such σ field, since we have the exact leading mass dependence of the free energy. The above result is also numerically compatible with the condensate obtained from the large-N framework in [21], which relies on a saddle-point approximation developed via the auxiliary field method and depends on a cutoff parameter. It agrees also with the result obtained to leading order in $1/N$ within the vector $O(N)$ model in [17,24].

Therefore, the quark condensate at this level of approximation vanishes at T_c and, more importantly, is not defined above T_c, unlike the ChPT expression, which is just a polynomial whose leading order is recovered just by expanding (17) in powers of T^2/T_c^2, namely, $\langle\bar{q}q\rangle(T)/\langle\bar{q}q\rangle(0)=1-T^2/(8F^2)+\cdots$; this corresponds to the leading order ChPT result in the chiral limit for $N=3$ [10,22]. Note also that, consistently with previous studies [22] T_c is independent of N to leading order. As for the particular value of the transition temperature T_c, taking the standard value for the pion decay constant in the chiral limit $\sqrt{N}F\simeq 87.1$ MeV yields $T_c\simeq 174.24$ MeV, which is high compared to the restoration temperature in the chiral limit expected from lattice data, which according to our comments in the introduction should be typically around $T_c\sim 120$ MeV. However, the present approach is not meant to provide a T_c close to such lattice values, mostly because it is based only on NGB degrees of freedom. Heavier states in the partition function contribute significantly to reduce the condensate and T_c [7,10,27]. In addition, higher order Lagrangians could modify the $T=0$ value of the condensate and hence the critical temperature. What is more meaningful is to compare the result (17) with the standard ChPT analysis to different orders in the chiral limit [10], as we show in Fig. 4.

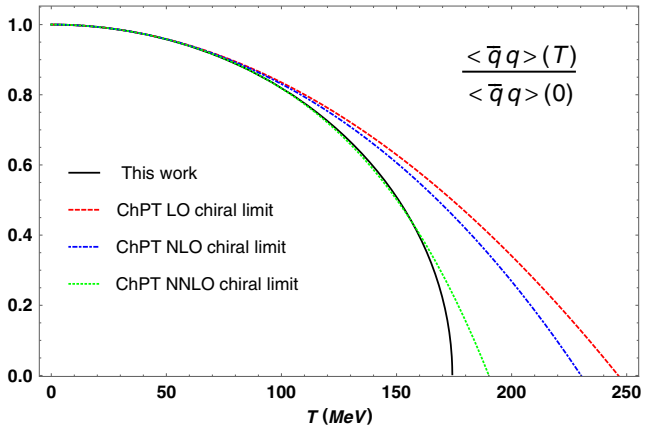

FIG. 4. Quark condensate in the large N in the chiral limit compared to the ChPT results for different orders as obtained in [10].

The value of T_c is reduced with respect to the next-to-next-to-leading order (NNLO) ChPT while being kept within the expected uncertainty given by a $1/N$ expansion near $N=3$. Actually, from the chiral expansion of (17) we get already a factor of $\sqrt{2}$ reduction in T_c with respect to leading order ChPT.

As discussed in the introduction, the main improvement of the large-N analysis with respect to the ChPT one is that the system undergoes a second-order phase transition, as corresponds to QCD in the chiral limit, which is clear from the analytic expression (17) and from Fig. 4. The system does not undergo a first-order phase transition since there are not jump discontinuities in the order parameter; the latter behavior is seen for instance when considering auxiliar field methods to analyze finite-temperature effects in an $O(4)$ nonlinear model [32]. This second-order critical behavior is confirmed by our analysis of the scalar susceptibility below.

Despite the fact that we cannot access from this approach the region $T>T_c$, let us analyze further the analytic behavior of the condensate (17) below T_c. At this point it is important to recall the critical behavior observed in lattice QCD. In [2], the scaling with the quark mass and the temperature of lattice data is fitted reasonably well to the

TABLE I. Critical exponents for different universality classes and the present analysis. We include for reference also the result obtained from saturating the susceptibility with the thermal $f_0(500)$ pole as discussed in [14,16] and in the main text. In that case, we use the results of the Grayer fit in that paper.

Model	β	γ_χ^-
Three-dimensional $O(2)$	0.35	0.49
Three-dimensional $O(4)$	0.38	0.54
This work	0.5	0.75
Saturated thermal pole large N [16]		0.975
Saturated thermal pole IAM [14]		1.005

three-dimensional $O(2)$ and $O(4)$ universality classes (see [33] for a review). Thus, the quark condensate is expected to scale in the chiral limit $m_q = 0$ as the second-order behavior $\langle \bar{q}q \rangle(T) \sim |T_c - T|^\beta$ for $T \to T_c^-$, where the value of the critical exponent β is given in Table I for the cases considered in [2]. Our value is then $\beta = 1/2$ from (17), which is not far from the lattice observations, still within the $1/N$ expected error, although giving a stronger critical behavior. Note that, as commented above, we are including only Goldstone bosons and not heavier states and hence we must consider our framework as a qualitative description of the transition, which actually captures its main critical features and certainly improves over standard low-T expansions such as ChPT. In fact, the critical behavior is meant to be controlled by Goldstone bosons below the transition [33].

In order to gain more insight into the above-mentioned critical features, let us now calculate the leading order contribution of the scalar susceptibility χ_S from the free-energy result (16), keeping only the leading term for $M \to 0^+$. After taking into account the mass expansion in (16) and the functions involved, we find the following remarkably simple expression:

$$\chi_S(M,T) = \frac{NTB_0^2}{4\pi M}\left(1 - \frac{T^2}{T_c^2}\right)^{-3/4} + \mathcal{O}(\log M, N^0). \quad (18)$$

Expression (18) diverges below T_c as a second-order phase transition, as QCD in the chiral limit, and confirming our previous analysis of the condensate. Actually, the critical behavior with T and M for $O(2)$ and $O(4)$ three-dimensional models is given by $\chi_S(M,T) \sim M^{-1}(T_c - T)^{-\gamma_\chi^-}$ for $T \to T_c^-$ and $M \to 0^+$, where the values of the critical exponent γ_χ^- are given in Table I. Therefore, we reproduce the expected mass behavior for χ_S and we obtain a critical exponent slightly above but not far from those models, which reproduce fairly well the critical behavior of lattice QCD [2]. As explained above, this is more than reasonable for a description based only on the lightest NGB, which again lies within the expected numerical uncertainty while capturing the main features of the chiral transition. Note also that, consistently, from (18) we recover the leading order ChPT expression for the thermal part of the susceptibility in the chiral limit [26,27] as $\chi_S = \frac{NTB_0^2}{4\pi M} + \cdots$. The $T = 0$ vanishes at this order and is included in the $\log M$ neglected corrections in (18).

Finally, we also compare our results with the analysis performed in [14] and [16], from which one can define a scalar susceptibility saturated by the thermal $f_0(500)$ state, with a mass corresponding to that scalar resonance defined as $M_S^2(T) = M_p^2(T) - \Gamma_p^2(T)/4$, where $s_p = (M_p - i\Gamma_p/2)^2$ is the position of the pole in the second Riemann sheet of the scattering partial wave with isospin and angular momentum $I = J = 0$ calculated also at finite temperature within the large-N limit in [16] and with the IAM in [14] around the chiral limit. In order for such saturated susceptibility to comply properly with the expected low-T behavior given by the leading order ChPT in the chiral limit, we define it as

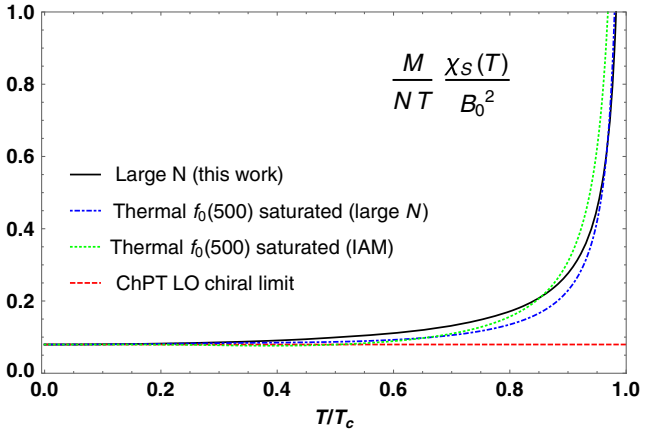

FIG. 5. Scalar susceptibility in the present approach compared to the thermal $f_0(500)$ saturated one defined through (19), considered in [16] at large N, where the results with the Grayer fit in that paper have been taken. We also include the saturated susceptibility with the IAM [14] in the chiral limit and the ChPT leading order chiral limit result for comparison. Temperatures are rescaled to the critical temperature for each case, namely, $T_c = 174.24$ MeV for the present approach, $T_c = 92.33$ MeV for the saturated large-N one, $T_c = 118.2$ MeV for the saturated IAM, and $T_c = 246.42$ MeV for the ChPT chiral limit one.

$$\chi_S^{sat}(T) = \frac{NTB_0^2}{4\pi M}\frac{M_S^2(0)}{M_S^2(T)}, \quad (19)$$

neglecting the $T = 0$ logarithmic contribution near $M \to 0^+$, and we plot $M\chi_S/(B_0^2 NT)$ for different approaches, which are then N independent. The results are shown in Fig. 5, where we also include the ChPT chiral limit one for comparison, which to leading order is just a constant with the normalization chosen. Higher order ChPT corrections yield smoothly growing functions of T. In the saturated large-N case, we have used the parameters of the so-called Grayer fit in [16].

First of all, we observe that the values of the critical temperature differ considerably between the free-energy analysis, like the one we present here or ChPT, and those based on thermal $f_0(500)$ saturation (either IAM or large N). As we have commented above, the numerical value of T_c obtained from the present approach is presumably affected by higher order terms and does not account for any physical state other than the NGB ones. In contrast, the saturation approach incorporates successfully the thermal $f_0(500)$, relying on a good description of the physical $T = 0$ pole consistent with scattering data and the quoted PDG values for that state. In fact, the critical temperature

of that approach is closer to the expected values from lattice analysis, which highlights the importance of that thermal state. Nevertheless, the most important result here has to do with the critical behavior, so that in order to provide a clearer comparison of the two approaches in that sense, we have represented the susceptibility in terms of T/T_c, where T_c is different for each method.

As it can be seen from Fig. 5, although the critical exponent for the saturated $\chi^{sat}(T)$ is larger (the numerical results are given also in Table I[2]), they depart later from the low-T ChPT value, so in the end the two approaches remain very close near the critical region. This is an important check of consistency between those two different ways to determine χ_S, concerning its critical behavior.

V. CONCLUSIONS

In this work we have analyzed the quark condensate and the scalar susceptibility of a gas of N Goldstone bosons to leading order in N in the chiral limit. Obtaining the leading behavior of the susceptibility requires computing up to M^3 corrections in the free energy (which come from an infinite set of closed ring diagrams). To this order, the results are directly finite and then it is no necessary to add higher order Lagrangian counterterms within the usual large-N framework. This diagrammatic treatment in terms of thermal effective vertices and dominant diagrams would allow us to extend this analysis beyond the chiral limit or for higher orders in the $1/N$ expansion.

Our results show a critical behavior in reasonable agreement with the universality classes expected for lattice simulations of the chiral transition, both for the quark condensate and for the scalar susceptibility, within the numerical uncertainties expected for a large-N approach. This is particularly realized in the critical exponents for those quantities. The quark condensate improves over NNLO ChPT in the sense that it reduces the value of its vanishing point and, more importantly, it behaves as the order parameter of a second-order transition, the critical T_c being N independent to leading order. The differences in the critical temperature with respect to ChPT remain within the expected $1/N$ uncertainty. Likewise, the scalar susceptibility that we have calculated here diverges at the same T_c as the condensate vanishing, as it should. In fact, another motivation of the present work was to test the consistency of a recent approach based on saturating the scalar susceptibility with the thermal $f_0(500)$ resonance pole. Our present analysis shows a reasonable agreement between the two methods regarding the critical behavior in terms of T/T_c. However, the value of T_c is much lower in the saturated approaches that in those based on the partition function, like ChPT or the one we present here. This is most likely due to having incorporated properly the physical $f_0(500)$ state and its thermal dependence, which somehow mimics the influence of higher order contributions in the perturbative chiral approach.

Obtaining higher order corrections in the mass expansion requires summing additional infinite sets of diagrams, the so-called foam diagrams. This is especially interesting for the case of the scalar susceptibility, since, in principle, it should lead to a change from a divergent second-order transition to a smooth peak characteristic of a crossover, as observed in lattice simulations. That analysis is beyond the scope of this work and will be analyzed elsewhere. Nevertheless, we believe that the present study can be useful as a first approach to this problem, setting up the diagrammatic framework for future studies while extending previous analysis in a nontrivial way and capturing the main features of chiral restoration in QCD.

[2]In the saturated cases, the critical exponents γ^- in Table I differ from those quoted in [16] by small numerical corrections that come from taking more points close to the transition temperature in the present work.

ACKNOWLEDGMENTS

Work partially supported by Contracts No. FPA2014-53375-C2-2-P and No. FIS2014-57026-REDT (Spanish Hadron Excelence Network) from the Spanish "Ministerío de Economia y Competitividad." We also acknowledge the support of the HadronPhysics3 project from the European Union Seventh Framework Programme (EU-FP7). S. Cortés thanks Professor José Rolando Roldán and the High Energy Physics group of Universidad de los Andes and Colombian "Departamento Administrativo de Ciencia, Tecnologia e Innovacion" (COLCIENCIAS) for financial support.

[1] Y. Aoki, S. Borsanyi, S. Durr, Z. Fodor, S. D. Katz, S. Krieg, and K. K. Szabo, J. High Energy Phys. 06 (2009) 088.

[2] S. Ejiri, F. Karsch, E. Laermann, C. Miao, S. Mukherjee, P. Petreczky, C. Schmidt, W. Soeldner, and W. Unger, Phys. Rev. D **80**, 094505 (2009).

[3] A. Bazavov, T. Bhattacharya, M. Cheng, C. DeTar, H. T. Ding, S. Gottlieb, R. Gupta, P. Hegde *et al.*, Phys. Rev. D **85**, 054503 (2012).

[4] T. Bhattacharya, M. I. Buchoff, N. H. Christ, H.-T. Ding, R. Gupta, C. Jung, F. Karsch, Z. Lin *et al.*, Phys. Rev. Lett. **113**, 082001 (2014).

[5] R. D. Pisarski and F. Wilczek, Phys. Rev. D **29**, 338 (1984).
[6] J. Berges, N. Tetradis, and C. Wetterich, Phys. Rep. **363**, 223 (2002).
[7] A. Tawfik and D. Toublan, Phys. Lett. B **623**, 48 (2005).
[8] P. Huovinen and P. Petreczky, Nucl. Phys. **A837**, 26 (2010).
[9] J. Gasser and H. Leutwyler, Ann. Phys. (N.Y.) **158**, 142 (1984).
[10] P. Gerber and H. Leutwyler, Nucl. Phys. **B321**, 387 (1989).
[11] A. Gomez Nicola, F. J. Llanes-Estrada, and J. R. Pelaez, Phys. Lett. B **550**, 55 (2002).
[12] A. Dobado, A. Gomez Nicola, F. J. Llanes-Estrada, and J. R. Pelaez, Phys. Rev. C **66**, 055201 (2002).
[13] D. Fernandez-Fraile and A. Gomez Nicola, Eur. Phys. J. C **62**, 37 (2009).
[14] A. Gomez Nicola, J. Ruiz de Elvira, and R. Torres Andres, Phys. Rev. D **88**, 076007 (2013).
[15] A. Heinz, S. Struber, F. Giacosa, and D. H. Rischke, Phys. Rev. D **79**, 037502 (2009).
[16] S. Cortés, A. Gómez Nicola, and J. Morales, Phys. Rev. D **93**, 036001 (2016).
[17] A. Patkos, Z. Szep, and P. Szepfalusy, Phys. Lett. B **537**, 77 (2002).
[18] T. Appelquist and C. W. Bernard, Phys. Rev. D **23**, 425 (1981); L. Tataru, Phys. Rev. D **12**, 3351 (1975).
[19] A. Dobado and J. R. Pelaez, Phys. Lett. B **286**, 136 (1992).
[20] A. Dobado and J. Morales, Phys. Rev. D **52**, 2878 (1995).
[21] H. Meyer-Ortmanns, H. J. Pirner, and B. J. Schaefer, Phys. Lett. B **311**, 213 (1993).
[22] A. Bochkarev and J. I. Kapusta, Phys. Rev. D **54**, 4066 (1996).
[23] S. Jeon and J. I. Kapusta, Phys. Rev. D **54**, 6475 (1996).
[24] J. O. Andersen, D. Boer, and H. J. Warringa, Phys. Rev. D **70**, 116007 (2004).
[25] J. Zinn-Justin, *Quantum Field Theory and Critical Phenomena*, 4th ed. (Oxford University Press, Oxford, 2002).
[26] A. V. Smilga and J. J. M. Verbaarschot, Phys. Rev. D **54**, 1087 (1996).
[27] A. Gomez Nicola, J. R. Pelaez, and J. Ruiz de Elvira, Phys. Rev. D **87**, 016001 (2013).
[28] L. Dolan and R. Jackiw, Phys. Rev. D **9**, 3320 (1974).
[29] I. T. Drummond, R. R. Horgan, P. V. Landshoff, and A. Rebhan, Nucl. Phys. **B524**, 579 (1998).
[30] J. I. Kapusta and C. Gale, *Finite-Temperature Field Theory: Principles and Applications* (Cambridge University Press, Cambridge, 2006).
[31] P. B. Arnold and O. Espinosa, Phys. Rev. D **47**, 3546 (1993); P. B. Arnold and O. Espinosa, Phys. Rev. D **50**, 6662(E) (1994).
[32] E. Seel, S. Struber, F. Giacosa, and D. H. Rischke, Phys. Rev. D **86**, 125010 (2012).
[33] A. Pelissetto and E. Vicari, Phys. Rep. **368**, 549 (2002).